2024 International Conference on Unmanned Aircraft Systems (ICUAS)
June 4-7, 2024. Chania, Crete, Greece

Hybrid Locomotive Behaviors for an Amphibious Fixed-Wing / VTOL Tiltrotor UAV

Stephen J. Carlson*, Christos Papachristos

Abstract— **The theory and implementation of a set of alternate auxiliary locomotion modes are presented for an amphibious fixed-wing VTOL UAV. In real-world conditions and unstructured environments, the ability for the vehicle to employ alternative modes of locomotion is essential. By using tilting propulsor nacelles for thrust vectoring, the aircraft is able to taxi, or ferry, on the water surface. The VTOL tail motor is used for self-righting when the vehicle is unintentionally overturned. Equivalent comparisons to wheeled-robot maneuverability and controllability are provided. A set of experimental demonstrations are conducted, including an alternative to normal flight by using ground-effect for improved power efficiency.**

I. INTRODUCTION

Micro Aerial Vehicle (MAV) robots have proven their operational versatility across domains such as search and rescue, industrial operations, and exploration of unknown environments [1–8] by integrating advanced autonomy and resilient perception pipelines [9–12]. However, the prime imperative of any mobile robotic system is locomotive ability. It therefore follows that increasing the number of locomotive modes in a robot improves its utility.

Extending the line of our prior work related to Solar-VTOL migratory recurrent missions [13–15], using the MiniHawk-VTOL [16–18], we have designed, built, tested and tuned a novel robotic aircraft, the Gannet Solar-VTOL [19], capable of operating in wet environments, with the ability to hover for take-off and landing, and to transition into and out of fixed-wing forward-flight, allowing for efficient and effective traversal of a large volume of airspace. The morphology of the design consists of a swept delta wing providing lift for forward-flight, and three motors, or propulsors, mounted in a constellation around the center of mass. The rear (tail) motor only assists in hovering, while the pair of nacelle-mounted motors tilt using two servo mechanisms, providing for hovering and forward flight. Two additional servos control a pair of elevons. This minimal but operationally versatile [20, 21] configuration for enabling fixed-wing VTOL behavior is typically known as the Tricopter Tilt-Rotor (TTR) [22–26].

A byproduct of selecting this configuration is that it allows for exploring a set of alternate locomotive modes outside of the normal modes of fixed-wing forward-flight and hover. Specifically, these alternative locomotion options are as follows:

This material is based upon work supported by the NASA Award: *ULI: Robust and Resilient Autonomy for Advanced Air Mobility* and the NSF Award: *2008904: RI: Small: Learning Resilient Autonomous Flight*. The presented content and ideas are solely those of the authors.

The authors are with the University of Nevada, Reno, 1664 N. Virginia, 89557, Reno, NV, USA stephen_carlson@nevada.unr.edu

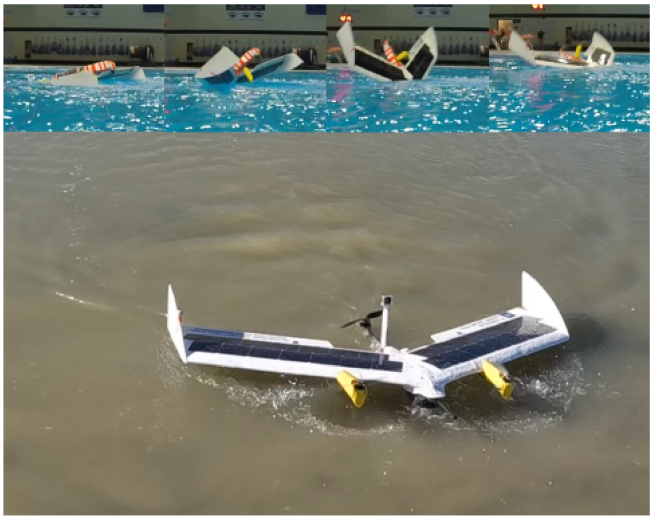

Fig. 1. Sequence of the Self-Righting Maneuver and Ferry behavior.

1) Surface repositioning, also termed “Taxi” or “Ferry”. This is useful for moving the aircraft short distances without committing to hovering flight.
2) Upset recovery from becoming inverted, termed “Self-Righting”. This capability is essential for the case in which the aircraft is rolled upside down by wind or wave action; without the ability to self-right, the aircraft is not able to take off or harvest solar power.
3) Near-surface reduced-power flight using Wing-in-Ground-Effect. By flying close to the water surface, the aircraft can enjoy higher power efficiency, but only where the sea state makes this viable, and where no other imperative to climb to altitude exists.

This paper shows the development of these alternate locomotive modes and their utility for the aircraft when operating in real-world environments, such as in high seas or nearshore docking and repositioning. These auxiliary modes of locomotion improve the capability of the aircraft, and in turn make it a more attractive platform for solving higher-level field robotics tasks.

This paper is organized as follows: Section II addresses related work. Section III shows the theory for using the propulsive elements of the aircraft for alternate motion behaviors. Section IV presents experimental results using the Gannet Solar-VTOL to ferry, self-right and fly in ground-effect. Finally, Section V summarizes the work presented.

II. RELATED WORK

The composite set of proposed auxiliary behaviors are drawn from two separate domains; Surface Locomotion

2024 International Conference on Unmanned Aircraft Systems (ICUAS) | 979-8-3503-5788-2/24/$31.00 ©2024 IEEE | DOI: 10.1109/ICUAS60882.2024.10557085

and Self-Righting are common features of wheeled robots, whereas Ground-Effect is a niche topic of manned and unmanned aircraft design. Relevant sources from both domains are reviewed below.

1) Surface Locomotion: The standard reference for wheeled robot mobility is [27]. In the field of aerial robotics, a distinct and early example of multi-mode mobility was the MMALV Project [28–32]. While the MMALV is a terrestrial-based flying robot, the principles of applying a wheeled-robot paradigm to a flying robot are relevant to our efforts. As to marine aerial robots, Eubank [33] shows a twin-engine seaplane design with differential-drive capability.

2) Self-Righting: Self-righting is shown in the Sherbrooke SUWAVE project [34, 35], using a single tilting nacelle with a range of rotation capable of elevating the propulsor out of the water for both the up-right and inverted aircraft pose cases. The "Dipper" [36] mentions a stabilization maneuver developed for that aerial-aquatic vehicle. Returning to [33], the "Flying Fish" did not make provisions for self-righting behavior, resulting in vehicle failure in at least one mission.

3) Ground-Effect Flight: Ground-effect vehicles and Ekranoplan aircraft are surveyed in [37]. Performance and design details for ground-effect-vehicles in [38] and [39] are referenced in this paper.

III. THEORY

This section addresses introduces the theory for each of the proposed behaviors. Subsection III-A demonstrates how the Gannet can be evaluated as a wheeled robot for the purposes of motion control and maneuverability when floating on a water surface. Subsection III-B constructs the flotation stability model of the Gannet and how the self-righting procedure introduces forces to overcome the static stability of the aircraft while inverted. Subsection III-C shows how the aircraft power requirements are reduced with the ground-effect phenomenon.

A. Water Surface Motion & Control Model

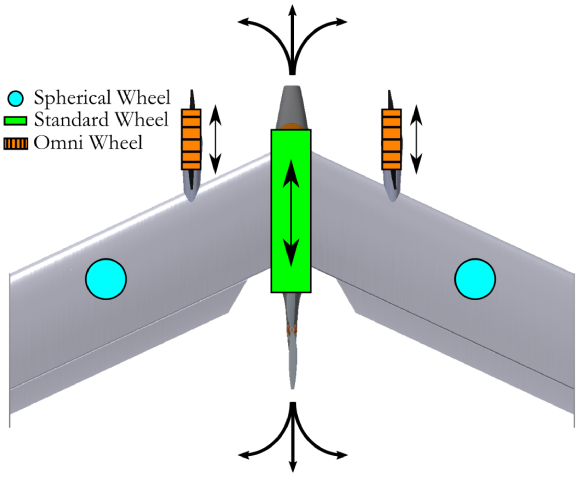

Fig. 2. Wheeled-Robot equivalent model. Only the "Omni Wheel" equivalent elements are powered, all other positions are analogies for unpowered rolling and sliding constrains.

On the water surface, the Gannet Solar-VTOL, or any other aircraft of similar configuration, can be modeled roughly as a differential-drive robot. This is arrived at as follows:

- The immediate ocean surface is defined as the local reference frame; all vehicle motion is with respect to this frame, or substrate.
- The long central body of the aircraft is always submerged when the vehicle is operating normally on the water surface. Given the central body shape and position, this can be modeled as a fixed wheel, with rolling constraints along the longitudinal axis of the aircraft, and sliding constraints along the lateral axis, due to the water drag resistance of any translational motion in the lateral direction.
- Accounting for the bulk interactions of the wing and other aircraft members floating on and interacting with the ocean substrate, outboard points on the left and right wings are modeled as spherical wheels with non-zero but negligible rolling resistance (drag).
- The two nacelle-mounted motors / propulsors can generate forces fore and aft in the longitudinal direction of the aircraft; these do not contribute sliding or rolling constraints, and are modeled as omni wheels with zero rolling resistance.

The equivalent wheeled-robot model is shown in Figure 2. This configuration has a degree of mobility equal to 2, and a steerability of zero, and thus a degree of maneuverability of 2. This is the same degree of maneuverability of a typical differential-drive robot, and so the Gannet can be controlled with the same control paradigm. The following equation resolves the movement of the Gannet in the global (world) reference frame:

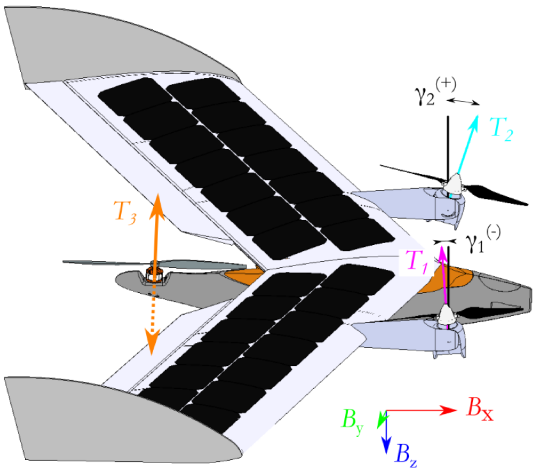

Fig. 3. Nacelle tilt angle conventions and rotor thrust descriptions.

$$\begin{bmatrix} \dot{x} \\ \dot{y} \\ \dot{\theta} \end{bmatrix} = \begin{bmatrix} cos(\theta) & 0 \\ sin(\theta) & 0 \\ 0 & 1 \end{bmatrix} \begin{bmatrix} u \\ r \end{bmatrix} \quad (1)$$

Where θ heading angle, x and y translation along the surface, u forward velocity, and r yaw axis angular rate. The

velocity and angular rate are roughly accumulated from the translational and rotational forces produced by the tilt rotor system, $\dot{u} = X/m$ and $\dot{r} = \tau/I_{zz}$, with m aircraft mass and I_{zz} aircraft rotational inertial along the vertical axis. The longitudinal force X and yaw torque moment τ come from:

$$\begin{bmatrix} X \\ \tau \end{bmatrix} = \begin{bmatrix} 1 & 1 \\ -d_{p_y} & d_{p_y} \end{bmatrix} \begin{bmatrix} T_1^{B_x} \\ T_2^{B_x} \end{bmatrix} \tag{2}$$

$$\begin{bmatrix} T_1^{B_x} \\ T_2^{B_x} \end{bmatrix} = \begin{bmatrix} T_1 \cdot sin(\gamma_1) \\ T_2 \cdot sin(\gamma_2) \end{bmatrix} \tag{3}$$

The thrusting forces $T_1^{B_x}$ and $T_2^{B_x}$ are expressed in the Body Fixed Frame, and modulated by the nacelle tilt angles γ_1 and γ_2. These elements are shown in Figure 3.

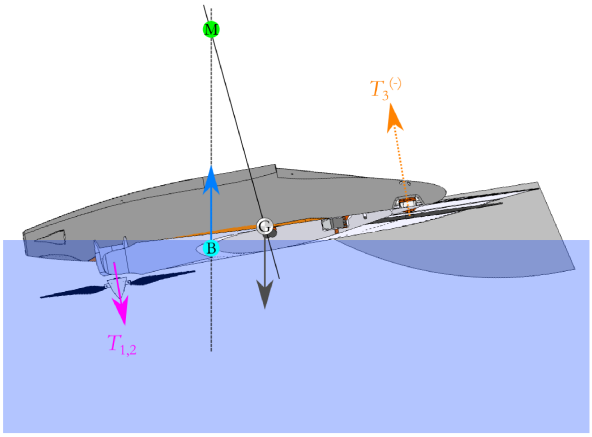

Fig. 4. Stability and forces in the self-right maneuver. M is the Metacentre, B Center of Buoyancy, G Center of Mass. Propulsor thrust vectors T_1, T_2, T_3.

B. Floating Longitudinal Motion

From marine architecture, the concept of the metacentre and metacentric height are used to articulate the stability of a floating shape such as a ship hull. In the case of when the Gannet is floating inverted in the water, the metacentric height is large, and therefore the aircraft is highly stable. This means that for any angular displacement from level equilibrium, the center of buoyancy quickly migrates away from the center of mass, resulting in a restoring torque moment. In order to flip the aircraft back over to upright, this restoring moment must be overcome with an opposite torque of greater magnitude. This is accomplished by configuring the the tail propulsor to produce a negative thrust force, and also asserting the forward nacelle-mounted propulsors to pull in a complementary direction. The combination of these forces overcomes the restoring moment, and the aircraft pitches up at a positive rate until fully turned back upright. Figure 4 shows the forces and metacentre.

C. Forward-Flight Aerodynamics & Ground-Effect

Ground-effect is the combination of an increase in lift and decrease in drag as the wing comes into proximity to a fixed surface. This comes from two different interactions. The first is Chord-Dominated Ground-Effect, or ram effect, which is produced by the interaction with the air under the wing as

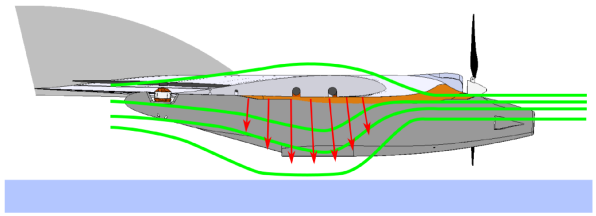

Fig. 5. Exemplified diagram of Wing-in-Ground-Effect phenomenon. Streamlines shown in green, pressure distribution in red.

it is compressed with the water surface. This increases the lift on the wing by augmenting the pressure distribution underneath. The second interaction, Span-Dominated Ground-Effect, is a drag-reduction phenomenon that results from the wingtip vortices being abated due to the proximity to the water surface. This can be interpreted as a slight extension of the wingspan, increasing the effective aspect ratio and the accompanying reduction in induced drag. Both of these interactions result in an improved L/D ratio, increasing the flight efficiency of the aircraft [39].

A side-effect of flying in ground-effect is that the longitudinal dynamics of the aircraft are altered. The reason for this is due to the center of pressure migrating as the aircraft wing comes into proximity to the water surface and produces ram pressure. Figure 5 shows a diagram of the air streamlines and pressure distribution when in proximity to the surface. This interaction typically results in oscillations in pitch and height. Various schemes are used to produce static longitudinal stability in purpose-designed ground-effect vehicles, such as reversed-delta wing and tandem-wing configurations [37]. However, as the Gannet Solar-VTOL was designed to be an out-of-ground-effect aircraft, no accommodations for ground-effect flight were made; i.e. the ability to fly at the ocean surface in ground-effect is incidental to the original design. In this regard, our aircraft is classed as a flying-wing / delta-wing in the classification system of [37]. This class typically has poor static longitudinal stability without augmentation by automatic control systems. At this time, we omit the identification of the longitudinal dynamics, or design of a controller for holding an optimal altitude above the surface, and leave this to later treatment.

Estimating the performance enhancement of flying in ground effect is generally tricky, but can be approximated as follows. For the Span-Dominated Ground-Effect component, the reduction in the induced drag is shown by [40] to be:

$$\sigma_{ge} = e^{-0.48(2H/b)^{0.768}} \tag{4}$$

with H height above the ground and b wingspan. σ_{ge} is also known as the ground-effect influence parameter. This can be used to find the effective aspect ratio in ground effect:

$$AR' = \frac{AR}{1 - \sigma_{ge}} \tag{5}$$

with AR the original aspect ratio of the wing. This can be used to find the modified induced drag of the aircraft,

$$C_{D_i} = \frac{C_L^2}{\pi e AR'} \tag{6}$$

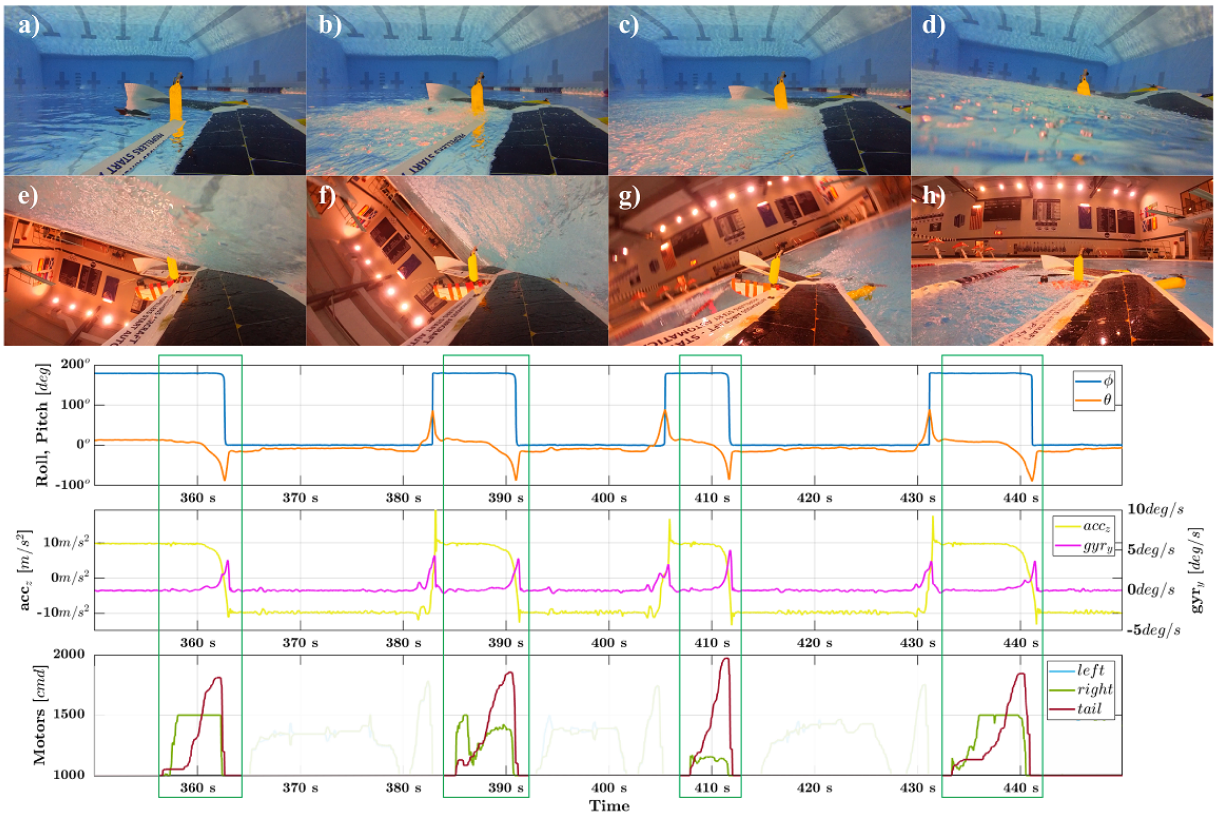

Fig. 6. Self-righting behavior. One instance of the maneuver is shown in the top portion, sequence a through h. The lower section shows multiple successful self-right maneuvers from the same session, with each event labeled within the green rectangles.

The Chord-Dominated Ground-Effect component is strongly coupled to the geometry of the entire vehicle, and is difficult calculate analytically. The main parameter is the height-to-chord ratio H/c; this has an asymptotic effect on C_L as the ratio decreases below 0.1. For the purposes of this analysis, given that the mean wing chord of the Gannet is $0.35m$, the Chord-Dominated contribution to improved lift is ignored.

Assuming that a value for the improved L/D can be found, this can be inserted into the electric form of the Breguet range equation:

$$R = (\frac{e_{bat}}{g})(\frac{\eta}{M_{tot}})(\frac{L}{D}) \tag{7}$$

where R range in meters, e_{bat} total battery energy, g gravity, η total drive efficiency, and M_{tot} total aircraft mass.

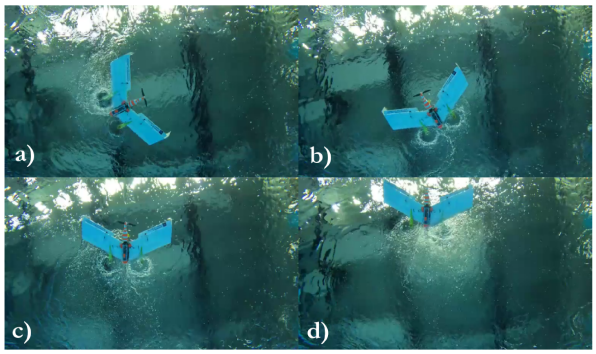

Fig. 7. Ferry motion sequence. (a, b) The aircraft turns 90 degrees. (c, d) The aircraft then proceeds to reverse on its tail backwards.

The improved performance will manifest as increased range of the aircraft. Or by symmetry, if the aircraft can be flown consistently in ground effect, the improved L/D can be determined via the difference in effective range.

IV. IMPLEMENTATION

With the properties and conditions established for the auxiliary movement modes, this section explains how each behavior is demonstrated in real-world testing.

A. Differential Drive Mobility

A standard handheld remote control unit is used to demonstrate the differential drive mobility of the aircraft. Propulsor thrust and nacelle tilt setpoints are mixed based on command stick positions. To establish movement, a moderate thrust level is commanded from a stick on the controller, and then forward-back and left-right inputs are mixed from a second gimbal. Figure 7 shows the view from below the aircraft while it is being commanded to perform turning and translating movement in the forward and reverse direction.

B. Upset Recovery with Self-Righting

The typical self-righting behavior is shown in Figure 6. The sequence starts with the aircraft fully inverted and resting stable on the water surface (a). The forward tilting propulsor pair have been rotated into the hover stance with respect to the aircraft body frame. In this stance, the pair are activated with a low requested throttle setpoint so as to provide a positive pitching torque moment, which tends

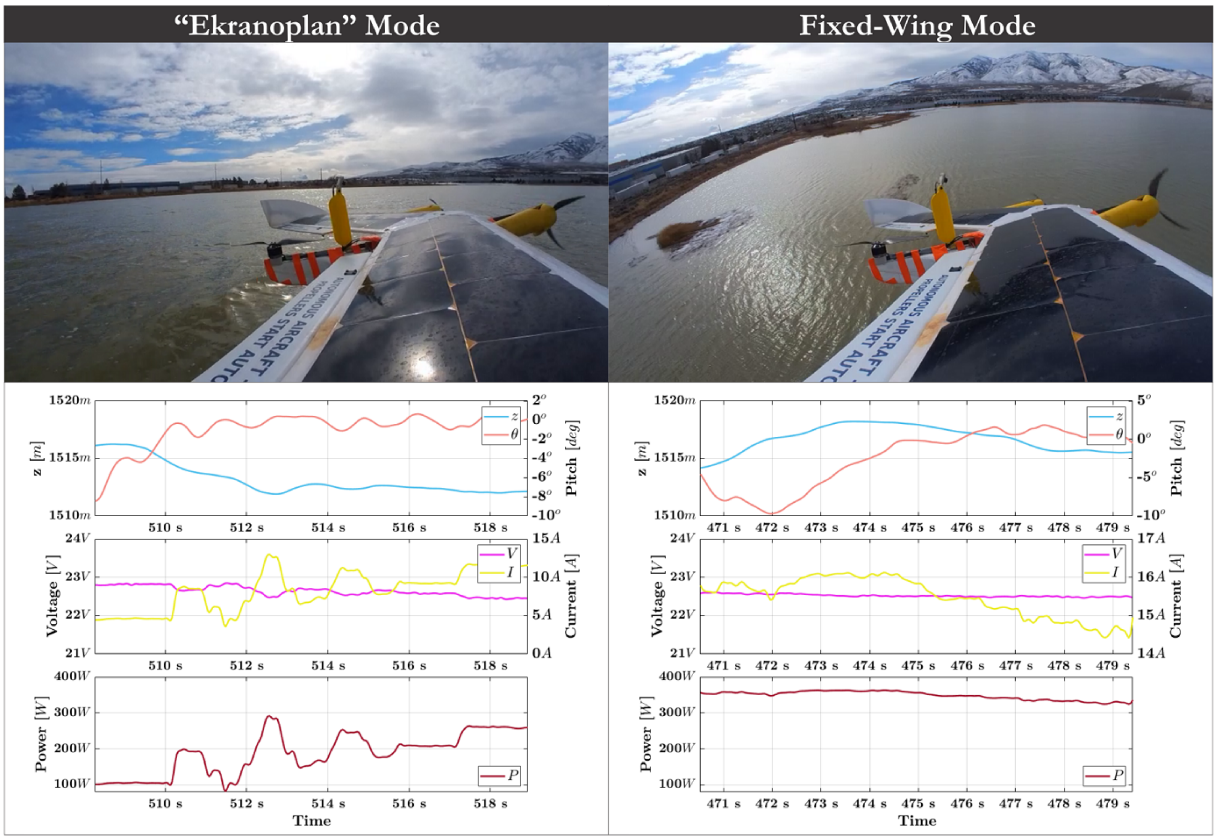

Fig. 8. Comparison of both forward-flight modes. Skimming the surface in "Ekranoplan" mode yields a fluctuating power estimate, averaging around $250W$ once flight is stabilized in ground-effect. During regular flight, the power requirements tends towards $300W$ or more in this case.

to bury the nose of the aircraft while simultaneously lifting the tail (b). When the tail has cleared the surface, the rear propulsor is activated in reverse thrust mode (c). While it is very inefficient to drive the propeller in reverse against the "spoon" of the blades, the force generated is sufficient to produce a positive pitch rate. The thrust setpoint on the tail propulsor is modulated to maintain a positive pitch rate until the aircraft has come over on its nose and continues until upright ($d-f$). The tail thrust setpoint is substantially attenuated or zeroed prior to completing the maneuver so as to prevent contact between the prop and the water surface (g, h). The forward propulsor pair may have also have the thrust setpoint increased but tend to only be employed to the degree necessary to pull the tail out of the water in the initial stage of the sequence.

The plot in the lower portion of Figure 6 shows a set of four consecutive self-right actions (indicated inside of the green rectangles), recorded in the same session as the image sequence. The first row shows the pose estimate, and the second row shows measured IMU values for vertical acceleration and aircraft pitch rate. The third row shows propulsor setpoints, and is transparency-masked to emphasize the upside-down to right-side-up transitions; the attenuated regions correspond to intentional repositioning and upside-down flips in the pool during testing.

C. Ground-Effect Flight

The ground-effect performance was found by flying the aircraft in fixed-wing forward-flight skimming above the surface of a lake in calm conditions. Figure 8 shows two instances during this test; one while skimming the surface the lake ("Ekranoplan" Mode), and another instance where the aircraft was at altitude out of ground effect. Only human (manual) control was available to keep the aircraft as close as possible to the water surface without contact, resulting in some ambiguity on the actual power requirement for flight in this mode. The plot in Figure 8 represents the cleanest sample captured, showing an estimated average power requirement of $250W$. Comparing to the out-of-ground-effect case of roughly $350W$ for sustained flight, a positive performance improvement appears to be present in this test. Follow-up testing with pitot-probe airspeed measurements and ground proximity feedback control can improve this metric.

V. CONCLUSIONS

This paper has shown a set of novel behaviors of an autonomous seaplane using the VTOL flight drive system for alternate modes of locomotion. The ability to navigate littoral (nearshore) and limnic (lake) regions is shown with the differential drive behavior. Vehicle self-righting using the same set of VTOL drive elements is demonstrated. Finally, an alternate forward-flight flight mode using ground-effect is shown, with resulting efficiency improvements. These hybrid behaviors aim to facilitate transoceanic autonomous flight.

REFERENCES

[1] T. Tomic, K. Schmid, P. Lutz, A. Domel, M. Kassecker, E. Mair, I. L. Grixa, F. Ruess, M. Suppa, and D. Burschka, "Toward a fully

autonomous uav: Research platform for indoor and outdoor urban search and rescue," *IEEE robotics & automation magazine*, vol. 19, no. 3, pp. 46–56, 2012.

[2] C. Papachristos and K. Alexis, "Augmented reality-enhanced structural inspection using aerial robots," in *2016 IEEE international symposium on intelligent control (ISIC)*. IEEE, 2016, pp. 1–6.

[3] G. Paul, S. Webb, D. Liu, and G. Dissanayake, "Autonomous robot manipulator-based exploration and mapping system for bridge maintenance," *Robotics and Autonomous Systems*, vol. 59, no. 7-8, pp. 543–554, 2011.

[4] C. Papachristos, F. Mascarich, S. Khattak, T. Dang, and K. Alexis, "Localization uncertainty-aware autonomous exploration and mapping with aerial robots using receding horizon path-planning," *Autonomous Robots*, vol. 43, no. 8, pp. 2131–2161, 2019.

[5] T. Dang, F. Mascarich, S. Khattak, H. Nguyen, N. Khedekar, C. Papachristos, and K. Alexis, "Field-hardened robotic autonomy for subterranean exploration," *Field and Service Robotics (FSR)*, 2019.

[6] C. Papachristos, S. Khattak, F. Mascarich, T. Dang, and K. Alexis, "Autonomous aerial robotic exploration of subterranean environments relying on morphology–aware path planning," in *International Conference on Unmanned Aircraft Systems (ICUAS)*, 2019, pp. 299–305.

[7] M. Tranzatto, F. Mascarich, L. Bernreiter, C. Godinho, M. Camurri, S. M. K. Khattak, T. Dang, V. Reijgwart, J. Loeje, D. Wisth, S. Zimmermann, H. Nguyen, M. Fehr, L. Solanka, R. Buchanan, M. Bjelonic, N. Khedekar, M. Valceschini, F. Jenelten, M. Dharmadhikari, T. Homberger, P. De Petris, L. Wellhausen, M. Kulkarni, T. Miki, S. Hirsch, M. Montenegro, C. Papachristos, F. Tresoldi, J. Carius, G. Valsecchi, J. Lee, K. Meyer, X. Wu, J. Nieto, A. Smith, M. Hutter, R. Siegwart, M. Mueller, M. Fallon, and K. Alexis, "Cerberus: Autonomous legged and aerial robotic exploration in the tunnel and urban circuits of the darpa subterranean challenge," *Field Robotics*, pp. 274–324, arXiv.2201.07 067, 2021.

[8] P. Arora and C. Papachristos, "Mobile manipulation–based deployment of micro aerial robot scouts through constricted aperture-like ingress points," in *2021 IEEE/RSJ International Conference on Intelligent Robots and Systems (IROS)*, 2021, pp. 6716–6723.

[9] S. Khattak, C. Papachristos, and K. Alexis, "Keyframe-based thermal–inertial odometry," *Journal of Field Robotics*, vol. 37, no. 4, pp. 552–579, 2020.

[10] S. Khattak, C. Papachristos, and K. Alexis, "Visual-thermal landmarks and inertial fusion for navigation in degraded visual environments," in *2019 IEEE Aerospace Conference*. IEEE, 2019, pp. 1–9.

[11] S. Khattak, F. Mascarich, T. Dang, C. Papachristos, and K. Alexis, "Robust thermal-inertial localization for aerial robots: A case for direct methods," in *2019 International Conference on Unmanned Aircraft Systems (ICUAS)*. IEEE, 2019, pp. 1061–1068.

[12] S. Khattak, C. Papachristos, and K. Alexis, "Marker based thermal-inertial localization for aerial robots in obscurant filled environments," in *Advances in Visual Computing: 13th International Symposium, ISVC 2018, Las Vegas, NV, USA, November 19–21, 2018, Proceedings 13*. Springer International Publishing, 2018, pp. 565–575.

[13] S. J. Carlson, P. Arora, T. Karakurt, B. Moore, and C. Papachristos, "Towards multi-day field deployment autonomy: A long-term self-sustainable micro aerial vehicle robot," in *2023 International Conference on Robotics and Automation (ICRA)*. IEEE, 2023.

[14] S. J. Carlson and C. Papachristos, "Solar energy harvesting for a land-to-recharge tiltrotor micro aerial vehicle," in *2022 IEEE Aerospace Conference (AERO)*, 2022, pp. 1–8.

[15] S. J. Carlson, T. Karakurt, P. Arora, and C. Papachristos, "Integrated solar power harvesting and hibernation for a recurrent-mission vtol micro aerial vehicle," in *2022 International Conference on Unmanned Aircraft Systems (ICUAS)*. IEEE, 2022, pp. 237–244.

[16] S. J. Carlson and C. Papachristos, "The MiniHawk-VTOL: Design, modeling, and experiments of a rapidly-prototyped tiltrotor uav," in *2021 International Conference on Unmanned Aircraft Systems (ICUAS)*. IEEE, 2021, pp. 777–786.

[17] S. J. Carlson and C. Papachristos, "Migratory behaviors, design principles, and experiments of a vtol uav for long-term autonomy," *ICRA 2021 Aerial Robotics Workshop on "Resilient and Long-Term Autonomy for Aerial Robotic Systems"*, 2021. [Online]. Available: https://www.aerial-robotics-workshop.com/uploads/5/8/4/4/58449511/icra2021-aerial_paper_8.pdf

[18] P. Arora, S. J. Carlson, T. Karakurt, and C. Papachristos, "Deep-learned autonomous landing site discovery for a tiltrotor micro aerial vehicle," in *2022 International Conference on Unmanned Aircraft Systems (ICUAS)*. IEEE, 2022, pp. 255–262.

[19] S. J. Carlson, B. Moore, T. Karakurt, P. Arora, T. Cooper, and C. Papachristos, "The gannet solar–vtol: An amphibious migratory uav for long–term autonomous missions," in *2023 International Conference on Unmanned Aircraft Systems (ICUAS)*. IEEE, 2023, pp. 419–424.

[20] C. Papachristos, K. Alexis, and A. Tzes, "Technical activities execution with a tiltrotor uas employing explicit model predictive control," *IFAC Proceedings Volumes*, vol. 47, no. 3, pp. 11 036–11 042, 2014.

[21] S. J. Carlson, P. Arora, and C. Papachristos, "A multi-vtol modular aspect ratio reconfigurable aerial robot," in *2022 International Conference on Robotics and Automation (ICRA)*. IEEE, 2022, pp. 8–15.

[22] C. Papachristos, K. Alexis, and A. Tzes, "Design and experimental attitude control of an unmanned tilt-rotor aerial vehicle," in *2011 15th International Conference on Advanced Robotics (ICAR)*. IEEE, 2011, pp. 465–470.

[23] C. Papachristos and A. Tzes, "Modeling and control simulation of an unmanned tilt tri-rotor aerial vehicle," in *2012 IEEE International Conference on Industrial Technology*. IEEE, 2012, pp. 840–845.

[24] C. Papachristos, K. Alexis, and A. Tzes, "Towards a high-end unmanned tri-tiltrotor: Design, modeling and hover control," in *2012 20th Mediterranean Conference on Control & Automation (MED)*. IEEE, 2012, pp. 1579–1584.

[25] C. Papachristos, K. Alexis, and A. Tzes, "Model predictive hovering-translation control of an unmanned tri-tiltrotor," in *2013 IEEE International Conference on Robotics and Automation*. IEEE, 2013, pp. 5425–5432.

[26] C. Papachristos, K. Alexis, and A. Tzes, "Dual–authority thrust–vectoring of a tri–tiltrotor employing model predictive control," *Journal of intelligent & robotic systems*, vol. 81, no. 3-4, pp. 471–504, 2016.

[27] R. Siegwart, I. R. Nourbakhsh, and D. Scaramuzza, *Introduction to autonomous mobile robots*. MIT press, 2011.

[28] R. Bachmann, F. Boria, P. Ifju, R. Quinn, J. Kline, and R. Vaidyanathan, "Utility of a sensor platform capable of aerial and terrestrial locomotion," in *Advanced Intelligent Mechatronics. Proceedings, 2005 IEEE/ASME International Conference on*. IEEE, 2005, pp. 1581–1586.

[29] R. Bachmann, R. Vaidyanathan, F. Boria, J. Pluta, J. Kiihne, B. Taylor, R. Bledsoe, P. Ifju, and R. Quinn, "A miniature vehicle with extended aerial and terrestrial mobility," *Flying Insects and Robots*, 2008.

[30] R. Bachmann, R. Vaidyanathan, and R. Quinn, "Drive train design enabling locomotion transition of a small hybrid air-land vehicle," in *Intelligent Robots and Systems, 2009. IROS 2009. IEEE/RSJ International Conference on*. IEEE, 2009, pp. 5647–5652.

[31] R. Bachmann, F. Boria, R. Vaidyanathan, P. Ifju, and R. Quinn, "A biologically inspired micro-vehicle capable of aerial and terrestrial locomotion," *Mechanism and Machine Theory*, vol. 44, no. 3, pp. 513–526, 2009.

[32] M. Polakowski, "An improved lightweight micro scale vehicle capable of aerial and terrestrial locomotion," Ph.D. dissertation, Case Western Reserve University, 2012.

[33] R. Eubank, E. Atkins, and G. Meadows, "Unattended operation of an autonomous seaplane for persistent surface and airborne ocean monitoring," in *OCEANS 2010 MTS/IEEE SEATTLE*, 2010, pp. 1–8.

[34] R.-A. Peloquin, D. Thibault, and A. L. Desbiens, "Design of a passive vertical takeoff and landing aquatic uav," *IEEE Robotics and Automation Letters*, vol. 2, no. 2, pp. 381–388, 2016.

[35] É. Tétreault, D. Rancourt, and A. L. Desbiens, "Active vertical takeoff of an aquatic uav," *IEEE Robotics and Automation Letters*, vol. 5, no. 3, pp. 4844–4851, 2020.

[36] F. M. Rockenbauer, S. Jeger, L. Beltran, M. Berger, M. Harms, N. Kaufmann, M. Rauch, M. Reinders, N. R. Lawrance, T. Stastny *et al.*, "Dipper: A dynamically transitioning aerial-aquatic unmanned vehicle." in *Robotics: Science and Systems*, 2021, pp. 12–16.

[37] K. V. Rozhdestvensky, "Wing-in-ground effect vehicles," *Progress in aerospace sciences*, vol. 42, no. 3, pp. 211–283, 2006.

[38] E. Cui and X. Zhang, "Ground effect aerodynamics," *Encyclopedia of Aerospace Engineering*, vol. 1, no. Part 3, pp. 245–256, 2010.

[39] A. Ghafoor, "Wing in ground effect vehicle: modelling and control," Master's thesis, Middle East Technical University, 2015.

[40] J. Wetmore and L. Turner Jr, "Determination of ground effect from tests of a glider in towed flight," NATIONAL AERONAUTICS AND SPACE ADMINISTRATION, Tech. Rep., 1940.